ELSEVIER

Chemical Geology 208 (2004) 247–264

CHEMICAL GEOLOGY
INCLUDING
ISOTOPE GEOSCIENCE

www.elsevier.com/locate/chemgeo

The formation of Pt–Ir alloys and Cu–Pd-rich sulfide melts by partial desulfurization of Fe–Ni–Cu sulfides: results of experiments and implications for natural systems

Anna Peregoedova[a,*], Sarah-Jane Barnes[b], Don R. Baker[a]

[a] *Earth and Planetary Sciences, McGill University, 3450 University Street, Montreal QC, Canada H3A 2A7*
[b] *Sciences de la Terre, Université du Québec à Chicoutimi, Chicoutimi, Canada G7H2B1*

Abstract

We propose a model of high-temperature formation of platinum-group element (PGE) alloys from base–metal sulfides subjected to decreasing sulfur fugacity (fS_2). For this purpose we experimentally investigated the effect of partial desulfurization of monosulfide solid-solution (Mss) with variable Ni and Cu contents on the distribution behaviour of Pt, Ir and Pd at 1000 °C. We partially removed sulfur from the PGE-bearing Mss using the "tube-in-tube" technique and pyrrhotite as an fS_2 buffer. We found that Mss undergoing S loss can produce (1) Pt and Ir exsolution from the Mss matrix in the form of PGE-bearing alloys, (2) partial melting of the Cu–Ni-bearing Mss to form Fe-rich Mss, Cu–Ni–Pd-rich sulfide liquid and Fe–Ir–Pt alloy. Both of these processes are geologically important. The partial melting of the S-depleted sulfides could explain the presence of two types of sulfides found in the mantle, Mss-dominated sulfides and S-poor sulfides consisting mainly of pentlandite and chalcopyrite. We also suggest that the Cu–Ni–Pd-rich liquid formed by partial melting of the sulfides could migrate away from the Mss and Fe–Ir–Pt alloys thus spatially decoupling Ir–Pt and Cu–Pd as observed in reefs and mantle nodules. In addition, the formation of PGE alloys in response to the desulfurization processes potentially could occur (1) after pressure falls during transport of the basalt magma with entrained sulfide droplets; (2) after sulfur removal by S-undersaturated melts or fluids from PGE-enriched sulfide proto-ore; (3) after degassing of the sulfide droplets occurring in a sub-volcanic chamber and (4) as a result of sulfide interaction with chromite.

Keywords: Platinum; Iridium and palladium alloys; Sulfur fugacity; System Fe–Ni–Cu–S; Experiments

1. Introduction

The presence of platinum-group element (PGE) bearing alloys in sulfur-poor silicate rocks is still not well understood. The main questions are how and at what stages of ore-formation do the alloys crystallize? Because of the common association of PGE with base–metal sulfides, it is reasonable to consider the problems of platinum-group mineral (PGM) formation in close connection with the processes of crystallization and subsolidus re-equilibration in the Fe–Ni–Cu sulfide systems. In mantle rocks the base–metal sulfides are typically found as monosulfide solid-solution (Mss) which hosts most of the mantle's PGE (e.g., Lorand, 1989; Bulanova et al., 1996;

* Corresponding author. Tel.: +1-514-485-9496; fax: +1-514-398-4680.
E-mail address: aperegoe@eps.mcgill.ca (A. Peregoedova).

0009-2541/$ - see front matter © 2004 Elsevier B.V. All rights reserved.
doi:10.1016/j.chemgeo.2004.04.015

Pattou et al., 1996; Alard et al., 2000; Lorand and Alard, 2001). Numerous experimental studies have revealed the great capacity of pyrrhotite [$Fe_{1-x}S$] and monosulfide solid-solution [$(Fe,Ni,Cu)_{1-x}S$] to concentrate PGE at magmatic temperatures (Makovicky et al., 1986, 1988, 1990; Fleet and Stone, 1991; Ballhaus and Ulmer, 1995; Li et al., 1996; Makovicky and Karup-Møller, 1999, 2000). Furthermore, Makovicky et al. (1986, 1988) showed the low-temperature exsolution of PGE phases from originally PGE-saturated pyrrhotite as a result of the sharp decrease in solubility of PGE in pyrrhotite with lowering temperature. The same concept of low-temperature exsolution-induced formation of discrete PGE phases was developed later by Ballhaus and Ulmer (1995) for PGE dissolved in monosulfide solid-solution and by Peregoedova and Ohnenstetter (2002) for PGE dissolved in quaternary solid-solution Hz-Iss [$(Ni,Cu,Fe)_{3\pm x}S_2$]. Ballhaus and Ulmer (1995) reported that the solubility of Pt and Pd in pyrrhotite falls strongly with decreasing temperature and decreasing sulfur fugacity (fS_2). Based on this observation, these authors concluded that the base–metal sulfides of the Merensky reef may have exsolved PGE to temperatures below 100 °C.

Nevertheless, a number of geological situations may have existed where a significant decrease in sulfur fugacity could happen at an earlier, high temperature, stage of ore-formation. For example, Lorand and Conquéré (1983) interpreted the metal rich compositions of some pentlandite-dominated sulfide assemblages in mantle xenoliths from the Massif Central, France, as resulting from desulfurization of the monosulfide solid-solution under high-temperature, open-system conditions. In addition, the loss of S from sulfides can also occur during the course of partial melting of the mantle, after pressure falls during transport of the mantle-derived magma with entrained sulfide droplets or as a result of sulfide interaction with percolating S-undersaturated melts/fluids, or with surrounding minerals.

It has been shown experimentally that at a given temperature the solubility of platinum-group elements in pyrrhotite and monosulfide solid-solution drops rapidly towards S-poor compositions and reaches zero at troilite composition (Makovicky et al., 1986, 1988, 1990; Li et al., 1996; Barnes et al., 1997a,b; Makovicky and Karup-Møller, 1999, 2000; Majzlan et al., 2002). Therefore, the depletion of Mss in sulfur, which would occur under conditions of declining sulfur fugacity, might lead to formation of individual PGE alloys.

In the present study, we propose a model of high-temperature formation of PGE alloys from base–metal sulfides subjected to decreasing sulfur fugacity. For this purpose we investigated the effect of partial desulfurization of high-temperature monosulfide solid-solution with variable base–metal ratios on the distribution behaviour of PGE. Experiments were carried out in the system Fe–Ni–Cu–S doped with Pt, Ir and Pd at the temperatures of 980 or 1000 °C and with fS_2 buffered by pyrrhotite. In accordance with the earlier paper by Ballhaus and Ulmer (1995) on Pt and Pd solubilities in pyrrhotite, we found that sulfur fugacity plays an extremely important role in the formation of individual PGE minerals. Our sulfur-buffered experiments show that variation in fS_2 directly affects the bulk metal/S ratio of sulfide assemblages and leads to a change in the stable assemblages of base–metal sulfides and PGE phases. In addition, we demonstrate that 1) the S-loss from the monosulfide solid-solution can lead to its partial melting, producing a Cu–Ni-rich sulfide melt and changing completely the original PGE distribution pattern, and 2) PGM-exsolution from the monosulfide solid-solution can occur at magmatic temperatures. Finally, we show how our findings can be applied to natural PGE deposits.

The following abbreviations are used throughout the paper: Mss—monosulfide solid-solution; Iss—intermediate solid-solution; Po—pyrrhotite; Pn—pentlandite; Cp—chalcopyrite; L—sulfide liquid.

2. Experimental and analytical methods

The starting sulfide assemblages were synthesized in evacuated silica glass tubes by melting a mixture of pure elements at 1200 °C (iron wire 99.99%, nickel wire 99.995%, copper foil 99.99%, sulfur pieces 99.999%, platinum wire 99.99%, iridium powder 99.995% and palladium tube 99.99% from Johnson-Matthey). As Mss with a variable base–metal ratio is the dominant sulfide phase in the mantle and igneous crustal rocks, the starting compositions of the present experiments were chosen so that, the run products at

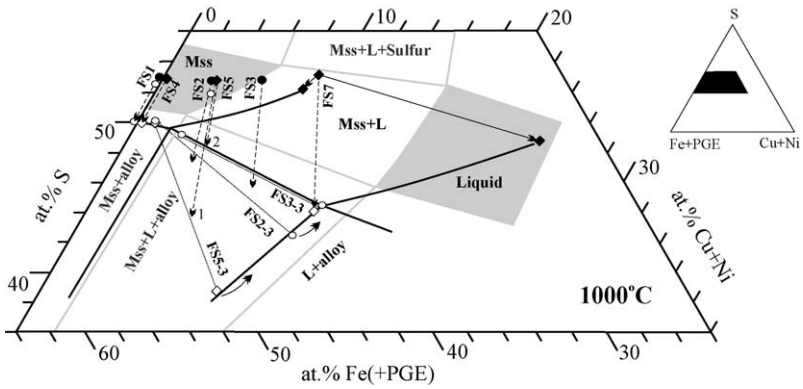

Fig. 1. Diagram showing schematically the displacement of the bulk compositions of the experimental runs across the phase fields of the system Fe–Ni–Cu–S at 980–1000 °C: solid circles and diamonds are the starting compositions with corresponding phase compositions for the experiments with Pt–Ir and Pd, respectively; open circles and diamonds are the compositions of the final products of the fS_2 buffering experiments with Pt–Ir or Pd, respectively; solid lines are the boundary between the phase associations according to the present experiments; shadowed fields are the same boundaries in more PGE-enriched systems (Li et al., 1996); dashed lines with arrows show the approximate shift of the sulfide composition with lowering sulfur fugacity; dotted lines are the tie-lines between coexisting Mss and sulfide liquid. See text for further discussion.

1000 °C would be either [Po], [Mss] or [Mss + liquid] (Li et al., 1996) (Fig. 1). The sulfur content of the starting samples was limited to approximately 53 at.%; Ni and Cu contents ranged from 0 to 4.5 at.%; sulfide samples were doped with platinum-group elements of 0.2 wt.% (0.05 at.%) each for Pt and Ir, and 0.5 wt.% (0.2 at.%) for Pd (Table 1).

The experiments were conducted following several methodologies. In the first series of experiments we investigated the final products of crystallization of PGE-bearing sulfide melts of the compositions of interest. These experiments were carried out with the sulfide samples slowly cooled from melting temperature (1200 °C) to room temperature with variable rates of cooling, from 6 to 30 °C/h, to investigate the PGM exsolution process on cooling. The aim of the second series of experiments was to synthesize base–metal sulfides with platinum-group elements in solid-solution. These experiments were performed with the same bulk compositions, but at 1000 °C followed by fast quenching in salted ice water to assure complete dissolution of all added PGE into the structure of base–metal sulfides. These PGE-bearing sulfides represent synthetic analogues of mantle sulfides and were used to model changes occurring under conditions of decreasing sulfur fugacity. In the course of these experiments sulfur fugacity was determined to evaluate fS_2 conditions at which a complete dissolution of PGE in sulfides of variable base–metal content occurs at magmatic temperatures.

Sulfur fugacity was estimated by the pyrrhotite indicator according to the equation of Toulmin and Barton (1964). Peregoedova and Ohnenstetter (2002) discussed the reliability of the method of Toulmin and

Table 1
Starting compositions

Run#	Wt.%							At.%						
	Fe	Ni	Cu	Ir	Pt	Pd	S	Fe	Ni	Cu	Ir	Pt	Pd	S
FS1	60.60			0.20	0.19		39.01	47.10			0.05	0.04		52.81
FS2	56.72	2.00	2.02	0.20	0.19		38.87	44.24	1.48	1.39	0.04	0.04		52.81
FS3	52.81	4.03	4.03	0.20	0.20		38.73	41.34	3.00	2.77	0.05	0.04		52.80
FS4	60.39					0.51	39.10	46.90					0.21	52.89
FS5	56.57	2.00	2.00			0.50	38.94	44.09	1.48	1.37			0.20	52.86
FS7	48.31	6.04	6.14			0.50	39.00	37.85	4.50	4.23			0.21	53.22

Barton (1964) for the fS_2 determination in the Fe–Ni–Cu–S system. We synthesized pyrrhotite of the composition approaching stoichiometric FeS and determined its composition and homogeneity by microscopic examination and X-ray diffraction (XRD). Then, an open silica-glass tube filled with Po powder was placed inside a larger tube filled with sulfide sample (in pieces) in such a manner that both the sample and the pyrrhotite coexisted with a common gas-phase but were not in physical contact with each other (Fig. 2A). In these experiments, the quantity of pyrrhotite powder was 30–40 times less than that of the main charge to prevent the influence of the Po composition on the composition of the sulfide sample via vapor phase. These "double tubes" were evacuated, sealed, annealed at 1000 °C for 5 days, and then quenched in salted ice water. In the course of annealing, the composition of pyrrhotite from the inner tube changed due to the exchange of sulfur vapor with the samples. The final composition of pyrrhotite was determined by both electron microprobe and X-ray diffraction by using its d_{102} value, and the $\log fS_2$ was calculated. A significant difference between fS_2 estimates by the two methods was observed (Table 2). This discrepancy is due to the difference in pyrrhotite composition obtained by electron microprobe and X-ray diffraction; the Po composition obtained by XRD method being more accurate. The electron microprobe analysis of the pyrrhotite was carried out in a wavelength-dispersion mode with a JEOL 8900 instrument at an accelerating voltage of 20 kV and a beam current of 30 nA. The counting time was 20 s. Synthetic FeS was used as standard for Fe and S in the samples FS1–FS3; synthetic $CuFeS_2$ was used also as standard for S in the samples FS4–FS7. The detection limits were 600–650 ppm for Fe and 220–300 ppm for S. Average standard deviation for Fe and S contents of Po determined by the electron microprobe is 0.15 wt.% with the maximum standard deviation attaining 0.27 wt.%. The uncertainty in the determination of Po composition by the electron microprobe is enough to significantly affect the fS_2 determination following the technique of Toulmin and Barton (1964) because fS_2 is extremely sensitive to the Fe/S ratio in the pyrrhotite. Reduction of the microprobe result for S content of pyrrhotite by only 0.15 wt.% reduces the calculated $\log fS_2$ by -0.95 at 1000 °C.

The diffraction peak {102} of the pyrrhotite was determined with a DRON-3 diffractometer, using Cu$K\alpha$ radiation and high-purity silicon powder as an external standard. The precision of the pyrrhotite composition determined by X-ray diffraction is ± 0.02 wt.% giving an error in calculated $\log fS_2$ of ± 0.03 at 1000 °C. According to Toulmin and Barton (1964), the total error in the estimate of $\log fS_2$ from pyrrhotite composition is about ± 0.35. In addition,

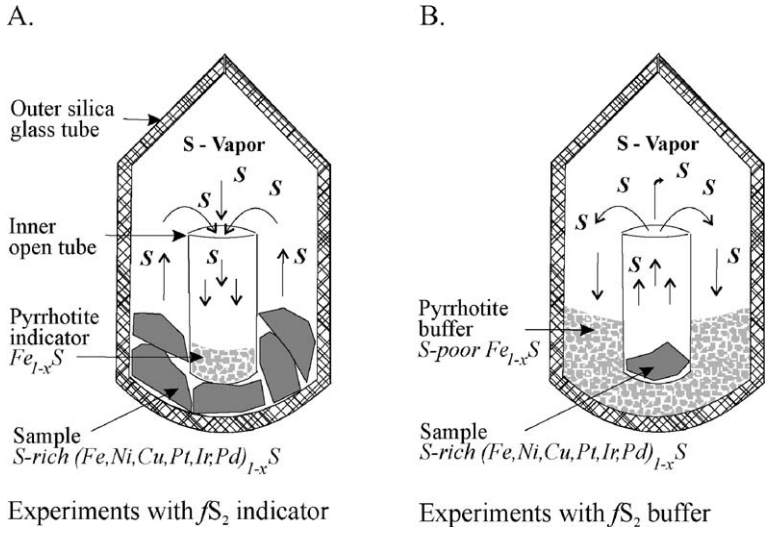

Fig. 2. Schematic of the "tube-in-tube" experiments where pyrrhotite is used as: (A) Indicator of the sulfur fugacity; (B) Buffer of the sulfur fugacity. See text for further discussion.

Table 2
Compositions of pyrrhotite with corresponding sulfur fugacity values

Run#	EMP data, wt.%			Log fS_2 by EMP	d_{102} of Po	Log fS_2 by XRD
	Fe	S	Total			
FS1-1 (1000 °C)	60.75	39.20	100.03	0.0	2.0708	−0.9
FS1-2 (1000 °C)	61.06	39.05	100.11	−0.3	2.0717	−1
FS1-3 (1000 °C)	63.23	36.90	100.13	−4.8	n.a.	
FS2-1 (980 °C)	60.67	39.05	99.72	−0.2	n.a.	
FS2-2 (980 °C)	61.37	39.10	100.47	−0.6	2.0722	−1.2
FS2-3 (980 °C)	63.85	36.85	100.70	−6.2	2.0948	<−7.1
FS3-1 (1000 °C)	60.71	39.05	99.76	−0.1	n.a.	
FS3-3 (1000 °C)	63.39	36.94	100.33	−4.9	2.0933	−6.7
FS4-1 (1000 °C)	61.14	39.51	100.66	0.0	n.a.	
FS4-3 (1000 °C)	63.56	37.12	100.67	−4.7	2.0955	<−6.9
FS5-1 (1000 °C)	61.09	39.64	100.73	0.2	n.a.	
FS5-3 (1000 °C)	63.56	37.18	100.74	−4.6	2.0932	−6.6
FS7-1 (1000 °C)	59.49	40.36	99.84	1.3	n.a.	
FS7-3 (1000 °C)	63.38	37.24	100.63	−4.2	2.093	−6.5

n.a.—not available. According to the results of XRD analyses for the Po buffer used in FS2-3 and FS4-3 its Fe/S ratio exceeds 1 and the equation of Toulmin and Barton (1964) is not applicable. For these samples we use the maximum log fS_2 (in atm.) corresponding to the composition of stoichiometric FeS (Fe/S = 1) at the temperature studied.

the pyrrhotite composition and corresponding sulfur fugacity determined by the method of X-ray diffraction are very close to the composition of pyrrhotites used as the fS_2 buffers in the same experiments. Because the pyrrhotite buffers were synthesized and weighed out on a high precision (0.0001 g) balance, their compositions are precise, thus the fS_2 deduced from the XRD determinations are more accurate. However, many runs produced insufficient pyrrhotite for XRD analysis, so for the relative change in log fS_2 the electron microprobe analyses have been used.

In the third series of experiments pyrrhotites with variable Fe/S ratio were used to reduce the sulfur fugacity of PGE-sulfides synthesized previously, and in this case the quantity of the Po buffer was 30–40 times larger than that of the sample (Fig. 2B). Two pyrrhotite buffers were used: FeS (63.5 wt.% Fe, 36.5 wt.% S) and $Fe_{0.9}S$ (61.2 wt.% Fe, 38.8 wt.% S). According to Toulmin and Barton (1964) the corresponding log fS_2 is expected to be respectively −6.8 and −0.6 at 1000 °C and −7 and −0.7 at 980 °C. The "tube-in-tube" assemblage was annealed at 1000 or 980 °C for 7 days and quenched in salted ice water. In the course of this annealing, the sample was equilibrated with the pyrrhotite buffer via the vapour phase leading to S reduction in the sample. This process of sulfur removal from the sample is an experimental model of a natural desulfurization process.

To confirm that the results obtained could be applicable to natural sulfides, some exploratory experiments were performed to test the possibility of PGE alloy formation in the S-poor pyrrhotite containing only trace quantities of Pt or Ir. For this purpose, pyrrhotites doped with 10 ppm of Pt or Ir were synthesized by mixing pyrrhotites initially containing 1000 ppm of the PGE with a stoichiometric FeS. The mixture was melted at 1250 °C and quenched in salted ice water to provide the best conditions for PGE solubility in the pyrrhotite structure (Cabri et al., 2003). The aim of this series of experiments was to examine whether individual PGE-bearing alloys will form at extremely low, close to natural, concentrations of platinum and iridium in the S-poor pyrrhotite. The few studies of PGE concentrations in natural pyrrhotites give ranges of 0.1–2.7 and 1.1–11.5 ppm or lower, for Pt and Ir, respectively (Ballhaus and Sylvester, 2000; Cabri et al., 2003).

The following method of naming the samples was used to identify the run conditions; FSX-Y, where X corresponds to the composition of the run; Y corresponds to the conditions of the run: with 0 = experiments with slow cooling of a sulfide liquid to room temperature to reveal final products of crystallization; 1 = quenched experiments with pyrrhotite indicator to determine the conditions of sulfur fugacity for the initial PGE-bearing sulfide association; 2 and 3 = experiments with pyrrhotite buffers to model the sulfur removal from PGE-bearing sulfide associations synthesized in the previous set of experiments.

Experimental durations of 5 to 7 days are sufficient to achieve equilibrium in the system Fe–Ni–Cu–S at a

temperature of 1000 °C, especially in the presence of sulfide liquid as in our Cu- and Ni-bearing experiments (Naldrett, 1967; Li et al., 1996). In our experiments, the sharpness of d_{102} peaks of the pyrrhotites is evidence that equilibrium was reached with respect to sulfur in the vapor in the course of annealing at 1000 °C. In addition, the compositions of base–metal sulfides and coexisting PGE phases were constant throughout the sample, providing another line of evidence for the attainment of equilibrium. The slow cooling experiments correspond to non-equilibrium conditions and the phase-relationships observed in these experiments cannot be attributed to a precise temperature.

The products of experiments were studied by the same electron microprobe used to analyse the pyrrhotite indicator. The sulfides $CuFeS_2$, FeS and $(Fe,Ni)_9S_8$ as well as Ni, Pt, Ir and Pd metals were used as standards. The analytical conditions were as follows: accelerating voltage 20 kV, beam current 30 nA, counting times up to 60 s, spot diameter of 3 μm. A defocused electron beam of 30 μm in diameter was used to determine the bulk compositions of sulfide liquid and base–metal sulfides containing exsolution-induced PGE phases when their size was too small to analyse individually. The detection limits for platinum-group elements were 600–1500 ppm, depending on counting time.

3. Results

The final products obtained after each series of experiments are shown in Table 3. Below we present first the phase relationships determined from quenched unbuffered experiments at 1000 °C (FSX-1 series) and continue with the description of the final products of crystallization of PGE-bearing sulfide liquids obtained in the slow-cooling experiments (series FSX-0). Finally, we will report results of the main experiments (series FSX-2,3) modeling the S loss from the PGE-bearing sulfides.

3.1. Results of the unbuffered experiments (FSX-1 series)

Except for run FS7-1, the starting compositions of most of the runs fall in the Mss [$(Fe,Ni,Cu,Pt,Ir,Pd)_{1-x}S$] field at 1000 °C (Fig. 1). Consequently, Mss is the only stable phase observed in the unbuffered quenched runs (Table 3). The starting composition of FS7-1 falls between liquid and Mss (Fig. 1) thus in the quenched run Mss and liquid were observed (Table 3).

Table 3
Results of experiments using pyrrhotite as fS_2 indicator or buffer

Run#	*T*, °C	Po	Log fS_2	Run products
FS1-0	SC	–	–	$Fe_{1-x}S$ + PtS
FS1-1	1000	indicator	−0.9	$(Fe,Pt,Ir)_{1-x}S$
FS1-2	1000	buffer 1	−1	$(Fe,Pt,Ir)_{1-x}S$
FS1-3	1000	buffer 2	"< −6.9"	$Fe_{1-x}S$ + Fe–Ir–Pt alloy
FS2-0	SC	–	–	Mss + Iss + Pt–phase
FS2-1	980	indicator	" −0.9"	Mss
FS2-2	980	buffer 1	−1.2	Mss + Pt–Ir ex.
FS2-3	980	buffer 2	< −7.1	Mss + L + Fe–Ir–Pt alloy
FS3-0	SC	–	–	Mss + Iss + Pt–phase
FS3-1	1000	indicator	" −0.9"	Mss
FS3-3	1000	buffer 2	−6.7	Mss + L + Fe–Ir–Pt alloy
FS4-0	SC	–	–	$Fe_{1-x}S$ + Pd–phase
FS4-1	1000	indicator	" −0.9"	$(Fe,Pd)_{1-x}S$
FS4-3	1000	buffer 2	< −6.9	$Fe_{1-x}S$ + Fe–Pd alloy
FS5-0	SC	–	–	Mss + Pd–phase
FS5-1	1000	indicator	" −0.9"	Mss
FS5-3	1000	buffer 2	−6.6	Mss + L
FS7-0	SC	–	–	Mss + Iss + Pd–phase
FS7-1	1000	indicator	"0.4"	Mss + L
FS7-3	1000	buffer 2	−6.5	L + Mss(?)

Buffer 1—Fe (61.2 wt.%), S (38.8 wt.%); Buffer 2—Fe (63.5 wt.%), S (36.5 wt.%); log fS_2 values (in atm.) given in commas were estimated by comparison with log fS_2 values determined by X-ray diffraction; SC—slow cooling.

The compositions of all run products are listed in Tables 4 and 5. Except for run FS7-1 all of the PGE dissolved into the Mss with no visible exsolution and the composition of the Mss is almost identical to that of the starting composition. In experiment FS7-1 Cu and Pd are strongly concentrated in the liquid relative to Mss, while Ni is slightly concentrated in the Mss (Table 5). The partition coefficients (Table 6) for these three elements between Mss and sulfide liquid are similar to those obtained in similar experiments by Li et al. (1996). The boundaries of the compositional fields of Mss and sulfide liquid are slightly (2–8 at.%) shifted toward Cu and Ni when compared with a similar diagram by Li et al. (1996). This is due to the much higher total concentration of PGE in their experiments (8 wt.% compared with 0.4–0.5 wt.% in the present experiments).

With the exception of run FS7-1, the log fS_2 calculated from the microprobe composition of the

Table 4
Compositions of phases in experiments with Pt and Ir

Run#	Phase	N	Composition, wt.%						
			Fe	Ni	Cu	Ir	Pt	S	Total
FS1-0 (SC)	$Fe_{1-x}S$	9	59.61 (0.27)			1.52 (0.17)	0.17 (0.03)	38.82 (0.15)	100.12 (0.28)
	PtS	6	1.33 (0.35)			< 0.2	83.71 (0.33)	14.22 (0.15)	99.30 (0.44)
FS1-1 (1000 °C)	$Fe_{1-x}S$	6	60.68 (0.19)			0.16 (0.01)	0.18 (0.03)	38.93 (0.1)	99.95 (0.24)
FS1-2 (1000 °C)	$Fe_{1-x}S$	7	61.02 (0.23)			0.18 (0.03)	0.17 (0.03)	38.81 (0.13)	100.18 (0.27)
FS1-3 (1000 °C)	$Fe_{1-x}S$	7	63.36 (0.18)			< 0.07	< 0.06	36.96 (0.1)	100.36 (0.21)
FS2-0 (SC)	Mss	7	57.79 (0.23)	2.25 (0.05)	0.92 (0.08)	0.21 (0.03)	< 0.06	39.17 (0.18)	100.35 (0.17)
	Iss	5	39.76 (0.96)	0.61 (0.14)	26.15 (1.21)	< 0.07	0.24 (0.14)	35.48 (0.45)	102.33 (0.89)
FS2-1 (980 °C)	Mss	8	57.09 (0.41)	1.97 (0.02)	3.14 (0.15)	0.15 (0.1)	0.19 (0.07)	38.48 (0.15)	101.02 (0.51)
FS2-2 (980 °C)	Mss	8	57.30 (0.28)	2.03 (0.01)	2.72 (0.12)	0.21 (0.07)	0.20 (0.07)	38.34 (0.1)	100.80 (0.35)
FS2-3 (980 °C)	Mss	6	62.26 (0.32)	0.41 (0.01)	1.29 (0.13)	< 0.07	< 0.06	36.73 (0.08)	100.72 (0.39)
	Fe–Ir–Pt	11	45.35 (0.61)	2.47 (0.11)	0.44 (0.11)	28.45 (0.53)	23.74 (0.61)	0.04 (0.03)	100.48 (0.35)
	Liquid	3	56.3 (1.19)	5.38 (0.51)	11.97 (2.29)	< 0.13	< 0.1	30.64 (0.67)	104.35 (1.39)
	Fe–Ni (q)	5	84.11 (1.00)	15.13 (0.85)	0.88 (0.06)	< 0.08	< 0.06	0.17 (0.08)	100.63 (0.5)
FS3-0 (SC)	Mss	6	55.55 (0.23)	4.48 (0.05)	0.85 (0.11)	0.23 (0.04)	< 0.06	39.34 (0.1)	100.44 (0.3)
	Mss + PGM	6	54.67 (0.11)	4.47 (0.08)	1.16 (0.20)	0.24 (0.05)	0.29 (0.13)	39.2 (0.15)	100.04 (0.28)
	Iss	7	39.85 (0.7)	0.61 (0.07)	25.77 (0.64)	< 0.07	< 0.06	35.37 (0.07)	101.83 (0.67)
FS3-1 (1000 °C)	Mss	7	53.72 (0.23)	3.98 (0.05)	4.41 (0.22)	0.17 (0.04)	0.17 (0.02)	38.46 (0.12)	100.91 (0.18)
FS3-3 (1000 °C)	Mss	6	61.84 (0.27)	0.78 (0.04)	2.97 (0.30)	< 0.07	< 0.06	36.38 (0.15)	101.98 (0.17)
	Fe–Ir–Pt	4	35.97 (0.2)	2.87 (0.02)	1.17 (0.3)	32.05 (0.46)	28.38 (0.54)	0.06 (0.04)	100.51 (0.4)
	Liquid	6	55.58 (0.8)	6.71 (1.22)	11.67 (1.92)	< 0.13	< 0.1	30.50 (1.47)	104.57 (1.04)

Here and elsewhere in tables: *N*—number of analyses to calculate the average composition; "< 0.06"—below the detection limit of the electron microprobe; numbers in parentheses are standard deviations; (q)—alloy formed from quenching of a liquid; Mss + PGM—due to the small grain size of exsolution-induced PGE phases in the matrix of Mss, a defocused beam was applied to analyze both Mss and PGE phases.

Table 5
Compositions of phases in experiments with Pd

Run#	Phase	N	Composition, wt.%					
			Fe	Ni	Cu	Pd	S	Total
FS4-0 (SC)	$Fe_{1-x}S$	9	60.56 (0.3)			0.10 (0.03)	38.86 (0.12)	99.80 (0.37)
	PGM (ex)	3	35.30 (8.79)			32.16 (11.75)	32.33 (2.03)	99.95 (0.9)
FS4-1 (1000 °C)	$Fe_{1-x}S$	8	60.47 (0.13)			0.53 (0.08)	38.64 (0.14)	99.93 (0.22)
FS4-3 (1000 °C)	$Fe_{1-x}S$	9	63.15 (0.24)			< 0.15	36.34 (0.12)	99.98 (0.24)
	Fe–Pd	6	30.93 (0.28)			67.06 (0.5)	2.25 (0.17)	100.46 (0.53)
FS5-0 (SC)	Mss	1	56.13	2.09	3.25	0.63	38.69	100.79
	Mss + PGM	3	53.61 (1.4)	2.05 (0.12)	2.61 (1.63)	3.48 (0.69)	37.90 (0.14)	99.66 (0.83)
FS5-1 (1000 °C)	Mss	10	56.79 (0.22)	2.08 (0.02)	2.44 (0.15)	0.54 (0.05)	38.31 (0.12)	100.16 (0.26)
FS5-3 (1000 °C)	Mss	10	62.24 (0.24)	0.64 (0.01)	0.86 (0.11)	< 0.09	36.30 (0.07)	100.07 (0.22)
	Liquid	14	57.60 (2.85)	7.25 (1.88)	5.54 (1.74)	3.46 (0.94)	26.03 (2.49)	99.88 (0.96)
	Fe–Ni–Pd (q)	3	56.81 (2.3)	24.22 (0.9)	2.96 (0.36)	16.92 (2.39)	1.43 (0.67)	102.33 (0.67)
FS7-0 (SC)	Mss	6	52.34 (0.4)	7.50 (0.11)	0.89 (0.26)	0.26 (0.05)	38.98 (0.13)	99.96 (0.34)
	Iss	15	38.14 (0.26)	1.15 (0.1)	24.72 (0.17)	< 0.09	34.93 (0.19)	99.07 (0.47)
	PGM (ex)	2	32.06 (3.87)	4.40 (1.12)	9.82 (4.22)	22.96 (2.45)	33.49 (0.79)	102.73 (0.88)
FS7-1 (1000 °C)	Mss	7	50.20 (0.23)	6.28 (0.02)	5.19 (0.11)	0.43 (0.08)	38.18 (0.12)	100.28 (0.26)
	Liquid	10	30.72 (1.51)	4.71 (1.2)	27.08 (1.8)	4.34 (1.76)	33.54 (0.31)	100.39 (0.64)
FS7-3 (1000 °C)	Liquid	14	52.18 (1.70)	7.85 (1.57)	9.01 (2.55)	0.79 (0.38)	30.54 (1.75)	100.37 (0.78)

Abbreviations are similar to those used in Table 3: PGM (ex)—exsolution-induced Pd-rich phase in a matrix of Mss (due to the small size of PGE phases the analyses can be used only to show that the composition was enriched in Pd).

Table 6
Mss/L partition coefficients for Ni, Cu and Pd

Run#	T, °C	S-content	D Mss/L		
		wt.%	Ni	Cu	Pd
FS2-3	980	<36.7	0.08 (0.01)	0.11 (0.02)	–
FS3-3	1000	<36.4	0.12 (0.02)	0.25 (0.05)	–
FS5-3	1000	<36.3	0.09 (0.02)	0.16 (0.05)	<0.03
FS7-1	1000	39	1.33 (0.34)	0.19 (0.01)	0.1 (0.04)

Numbers in parentheses are standard deviations of partition coefficients calculated according to the equation employed by Li et al. (1996).

pyrrhotite indicator is approximately 0 for all of these experiments in good accordance with very slight slope of fS_2 isobars in the Mss field in the system Fe–Ni–S reported by Naldrett (1967) (Table 2). The significant increase of sulfur fugacity observed in the sample richest in Cu and Ni, FS7-1, is due to the appearance of the sulfide liquid in the association with Mss. In addition, this agrees well with the data of Peregoedova and Ohnenstetter (2002), who have shown that at constant S content in the system Fe–Ni–Cu–S sulfur fugacity increases with the ratio of (Ni + Cu)/Fe. In spite of this high value of sulfur fugacity ($\log fS_2 = 1.3$) for FS7-1, our Po indicator still lies in the pyrrhotite compositional field, clearly below the S condensation curve at 1000 °C (Craig and Scott, 1974, and references therein). Moreover, as discussed above, the estimated $\log fS_2$ based on XRD of Po is more accurate and systematically lower than the estimates based on microprobe compositions. Unfortunately only one run, that richest in Fe, FS1-1, contained sufficient Po for XRD analysis. This gives an estimate of −0.9 for $\log fS_2$ (Table 2). Taking into account the similarity of fS_2 "microprobe" estimates for the samples FS1–FS5 and the practically horizontal slope of fS_2 isobars in the Mss field noted above, we can assume that $\log fS_2$ was close to −0.9 in all samples lying in the Mss compositional field (samples FS1–FS5), and that the real $\log fS_2$ in the sample FS7-1 was probably lower by 0.9 units than its "microprobe" determined value, which gives an estimate of 0.4 (Table 3).

3.2. Final products of PGE-bearing sulfide liquid crystallization (FSX-0 series)

The slow cooling experiments provide information about the textures formed when natural sulfide liquids crystallize. The run product of the Cu–Ni-poor runs consists of pyrrhotite with exsolutions of Pt or Pd phases (Tables 3–5). The run products of the Cu–Ni-bearing runs are Mss, Iss and exsolved phases with Pt or Pd. Based on phase diagrams for the Fe–Ni–Cu–S system (Kullerud et al., 1969) Mss was the first phase to crystallize and Iss represents the fractionated liquid. In most cases the Pt or Pd phases form as oriented lamellae hosted in the pyrrhotite or Mss matrix (Fig. 3A and B). The small size of the lamellae does not allow quantitative determination of their composition by microprobe; we can only confirm that they contain major amounts of Pt or Pd (Tables 4 and 5). Interestingly, no exsolution lamellae of Ir phases were found; this is consistent with the ability of Ir to substitute into the octahedral site of S-rich Mss (Barnes et al., 2001). In spite of the formation of exsolution-induced PGE phases, it was found that S-rich pyrrhotite (52.9 at.% S) contains high concentrations of Pd (0.1 wt.%), Pt (0.17 wt.%) and Ir (1.52 wt.%) when cooled slowly to room temperature (Tables 4 and 5). We find that Ni and Ir are enriched in Mss relative to the Iss, whereas Cu and Pt are enriched in the Iss relative to the Mss (Tables 4 and 5), consistent with Makovicky (2002).

We observed different morphologies of exsolved PtS in FS1-0 depending upon the cooling rate. In the most slowly cooled runs the exsolutions of PGE phases are lamellae. However, in FS1-0 some idiomorphic PtS grains of about 40 μm diameter were obtained by slow (~ 6 °C/h) cooling of PGE-bearing sulfide melt from 1210 °C to 300 °C (Fig. 3C). However, in the quench experiments FS1-1 only homogeneous pyrrhotite with Ir and Pt contents of 0.16 and 0.18 wt.%, respectively, is found (Table 4). These two observations suggest that Pt was dissolved at high temperature (1000 °C) in the pyrrhotite, but it exsolved from the Po structure in the form of PtS at lower temperature (FS1-0). The euhedral crystal shape obscures the exsolution-induced origin of PtS, demonstrating that subsolidus reequilibration and recrystallization could produce PGM crystals very similar to those crystallized directly from sulfide liquid. To investigate whether these grains are the product of recrystallization we modified the cooling rate of our experiments. Using the same composition and cooling the charge from 1000 °C to 300 °C in 1 day (~ 30 °C/h) yielded elongated lamellae exsolutions of PtS

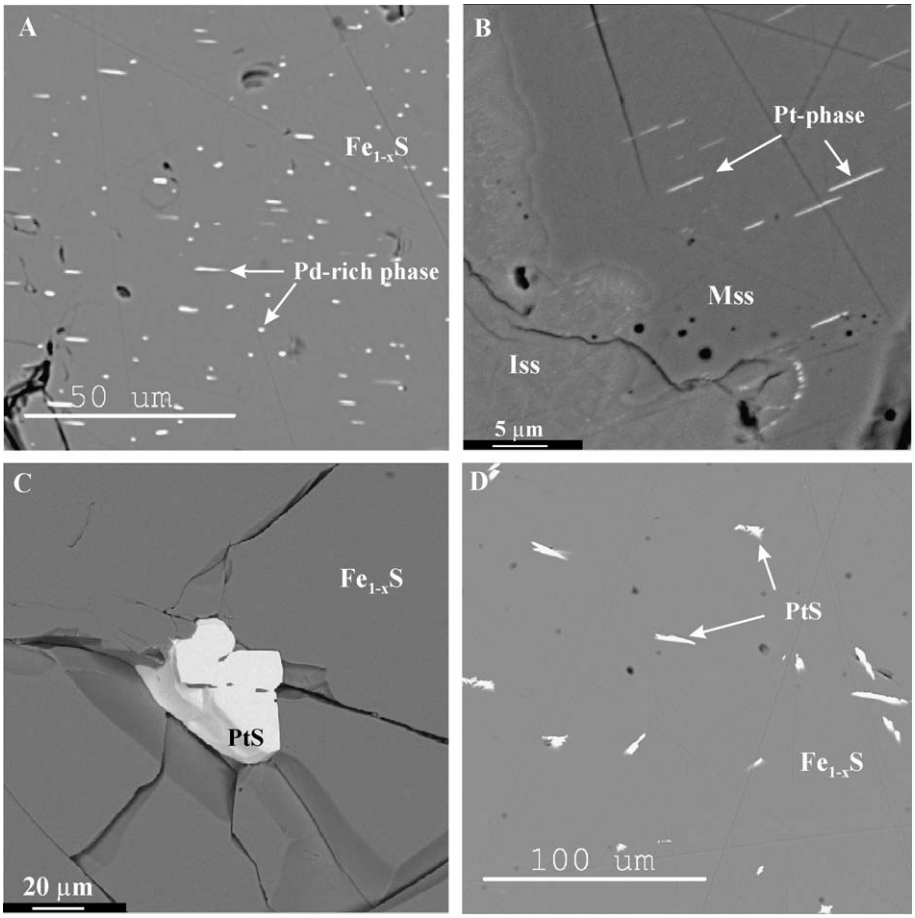

Fig. 3. Back-scattered electron images: (A) Exsolution-induced lamellae of the Pd-rich phase in the matrix of pyrrhotite formed during slow cooling of sample FS4-0; (B) Final products of crystallization of Cu–Ni bearing sulfide liquid including Mss with exsolution-induced lamellae of a Pt-rich phase and intermediate solid solution decomposed to different phases of the chalcopyrite family, run FS2-0; (C) PtS aggregate crystal formed from Pt-bearing pyrrhotite on slow cooling, run FS1-0; (D) PtS lamellae exsolved from Pt-bearing pyrrhotite on fast cooling, run FS1-6.

(Fig. 3D). In the latter case, the time was not sufficient for PtS exsolution-induced lamellae to grow by diffusion, and their exsolution texture is preserved. Therefore, care should be taken when using euhedral appearance of PGM grains as a proof of their early magmatic crystallization in natural sulfide ores.

According to the slow cooling experiments, the final products of crystallization of Cu–Ni-bearing sulfide liquid in the studied part of the system Fe–Ni–Cu–S consist of Iss and Mss hosting exsolution-lamellae of individual platinum (runs FS2-0, FS3-0) or palladium (runs FS5-0, FS7-0) phases. Apparently, the lamellae hosted by Cu- and Ni-bearing Mss (Fig. 3B) could not recrystallize to bigger grains due to their late, low-temperature exsolution. The reason for this is the higher PGE solubility in the Ni-bearing Mss (Li et al., 1996) compared with Ni-free pyrrhotite (Ballhaus and Ulmer, 1995) at the same temperature. Thus, exsolution-induced lamellae of PtS apparently formed in the pyrrhotite matrix at higher temperatures, and had time to recrystallize into bigger grains. This could also be due to variable diffusion speeds in different hosts, Po and Ni–Cu-rich Mss. To summarise, in Cu–Ni-bearing sulfide ores, the process of formation of secondary platinum-group minerals by exsolution from base–metal sulfides could be delayed in comparison with the same process occurring in sulfides enriched in Fe due to the higher solubility

limits of PGE in S-rich Mss typical for Cu–Ni-bearing associations (Peregoedova and Ohnenstetter, 2002).

3.3. Results of buffered experiments

The sulfur fugacity was reduced in experiments with the pyrrhotite buffers (FSX-2 and 3 series). The FSX-2 experiments (run in equilibrium with S-rich buffer) reduced log fS_2 only slightly as the S content of the Po buffer was close to the starting run compositions. Moreover, the reduction of log fS_2 by ~ 0.1–0.4 practically corresponds to or is even below the analytical uncertainty (Table 2). The FSX-3 experiments (run in equilibrium with the S-poor buffer) reduced log fS_2 by a much larger amount (~ 4.5–5.6) reducing the absolute value to, respectively, -6.5 and -7.1 (Table 2). The decrease in sulfur fugacity results in a partial transfer of sulfur from the sulfide to the vapor. Consequently the metal/sulfur ratio of the initial sulfides increased causing two important events: formation of PGE-bearing alloys and partial melting of the sulfides.

3.3.1. High-S buffered experiments (FSX-2 series)

Two experiments were run with the high-S buffer: FS1-2 at 1000 °C and FS2-2 at 980 °C. In both cases the run product was Mss (Table 3). The Pt and Ir contents of the Mss are close to the initial composition of the sample (0.2 wt.% of each element), thus most PGE are dissolved in the Mss. However, there are some very tiny exsolutions in FS2-2 at the boundaries of the grains of Mss (Fig. 4A). Microprobe analyses reveal elevated Pt and Ir concentrations in these areas but the precise composition cannot be determined due to the small grain size. In this case, the PGE phases reveal the following features: (1) formation of numerous separate grains of extremely small size (≈ 0.5 μm) and (2) occurrence in the most favorable, in terms of crystallography, position for exsolution-induced grains. It is very difficult to know if these grains were stable at run temperature or if they formed on quenching. However, no PGE phases appeared in the sample FS1-1 on quenching from 1000 °C in spite of almost identical fS_2 run conditions. Consequently at 980 °C, the first PGE phases might be appearing as exsolutions from the Mss containing about 0.2 wt.% Pt and Ir and the metal/S ratio (atomic) of about 0.93 when the log fS_2 decreases to approximately -1.2.

3.3.2. Low-S buffered experiments (FSX-3 series)

The two Cu–Ni free, low-S buffered experiments, FS1-3 and FS4-3, produced Po and PGE-bearing alloys. In the Pt–Ir doped experiments the alloy composition was not analysed due to its small size. Based on the data of Makovicky and Karup-Møller (2000), this alloy apparently is γ(Fe,Ir,Pt) solid-solution, with a composition dominated by Fe. The composition of alloy formed in experiments doped with Pd is very close to PdFe (Pd analogue of tetraferroplatinum PtFe) (Table 5). The Fe–Ir–Pt alloys occur as oriented lamellae in the pyrrhotite matrix (Fig. 4B). In contrast, the grains of the Pd–Fe alloy are mainly concentrated close to the boundaries with vapor phase as rounded relatively big blebs. The difference in texture is interpreted to indicate the higher mobility of palladium compared to platinum and iridium (Fig. 4C). The constancy of the Fe–Ir–Pt alloy composition through the samples, the relatively large size of some alloy lamellae (up to 5 μm in length), as well as the clear tendency of small grains to group together forming bigger grains (Fig. 4B), and the very big size (up to 17 μm) of the grains of Pd–Fe alloy (Fig. 4C) were taken as support for the equilibrium formation of PGE-bearing alloys in the low-S buffered experiments. No detectable amounts of Pt, Ir or Pd were found in the pyrrhotite matrix hosting the PGE-bearing alloys suggesting preferential distribution of the PGE into the metal phase (Tables 4 and 5).

Fig. 4. Back-scattered electron images: (A) Exsolution-induced Pt–Ir phase at the boundaries of the Mss grains after sulfur reduction of the Mss in run FS2-2, 980 °C; (B) Exsolution-induced lamellae of Fe–Pt–Ir alloy in a matrix of pyrrhotite appearing after reduction of fS_2 in run FS1-3, 1000 °C; (C) Grains of the Pd–Fe alloy formed by exsolution from pyrrhotite after reduction of fS_2 in run FS4-3, 1000 °C; (D) Partial melting of the Pt–Ir-bearing Mss caused by sulfur reduction and resulting in the formation of Cu–Ni-rich sulfide liquid (multiphase quench mixture) and PGE alloys (some of the bright crystals associated with a liquid) in run FS2-3, 980 °C; (E) Stable Fe–Ir–Pt alloy formed during partial melting of Mss, surrounded by Fe–Ni alloy formed from the liquid on quenching in run FS2-3, 980 °C; (F) Products of solidification of Cu–Ni–Pd sulfide liquid. The morphology of the grains of the Fe–Ni–Pd alloy (the brightest phase) is indicative of formation from a sulfide liquid on quenching and were not stable at run temperature, run FS5-3, 1000 °C.

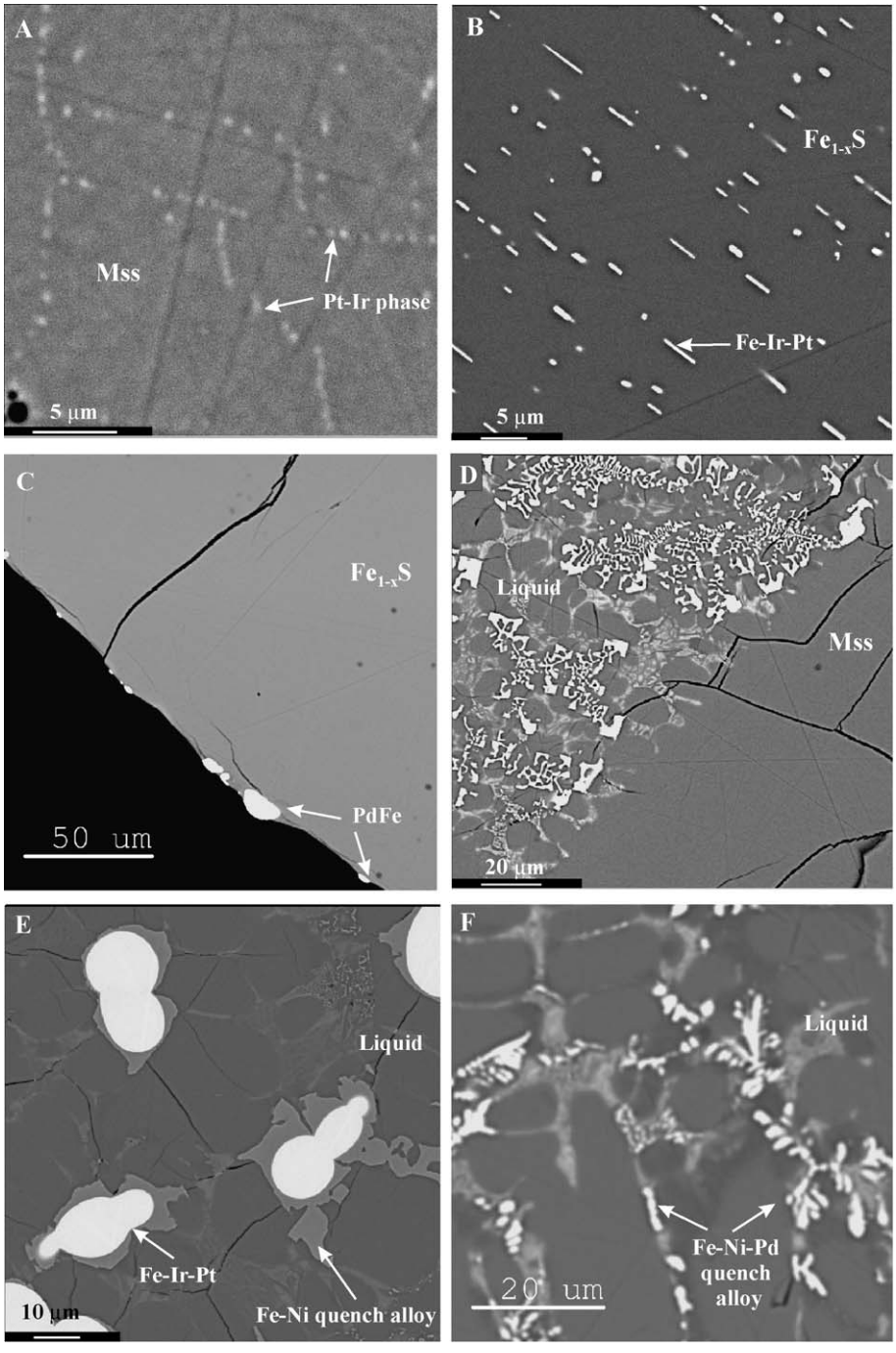
A
Mss
Pt-Ir phase
5 μm
B
$Fe_{1-x}S$
Fe-Ir-Pt
5 μm
C
$Fe_{1-x}S$
PdFe
50 um
D
Liquid
Mss
20 μm
E
Liquid
Fe-Ir-Pt
10 μm
Fe-Ni quench alloy
F
Liquid
Fe-Ni-Pd
quench
alloy
20 um

In the Cu–Ni-bearing experiments the run products were Mss, liquid and Fe–Ir–Pt alloy (Fig. 4D and E) in the Pt–Ir doped experiments, and Mss and liquid in the Pd doped experiments (Table 3). The Mss is depleted in Cu and Ni and Pd relative to the liquid. The incompatibility of Cu and Pd is similar to that observed at higher fS_2, but Ni shows a change in behavior from compatible at high fS_2 to incompatible at low fS_2. This change in behavior of Ni has been observed in previous experimental work (Barnes et al., 1997a,b; Makovicky, 2002) and the partition coefficients we found are similar to those reported previously for low fS_2. The composition of Fe–Ir–Pt alloy corresponds to the Fe-rich γ(Fe,Ir,Pt) solid-solution with a slight enrichment in Ir compared with Pt (Table 4).

The formation of alloy plus liquid is expected when the phase diagram is examined (Fig. 1). The reduction of sulfur in the system results in a shift of the bulk composition from within the compositional field of the monosulfide solid-solution through the field Mss + L to the three-phase association Mss + L + alloy for runs FS2-3, and FS3-3 (Fig. 1). During partial melting, the metal/sulfur ratio of the monosulfide solid-solution rises from 0.92 (in the sample FS2-1) to 1 (in the sample FS2-3), and all Pt and Ir dissolved originally in the S-rich Mss partition into the alloy leaving concentrations below our minimum detection limits in the S-poor monosulfide solid-solution (Table 4). A similar situation exists for sample FS3-3, but the Fe–Ir–Pt alloy formed in this sample is richer in Ir, Pt, Cu and Ni, and lower in Fe than the alloy formed in sample FS2-3 (Table 4).

The grains of primary Fe–Ir–Pt alloy are rather abundant and always bordered with Fe–Ni alloys formed on quenching of the sulfide liquid, making it very difficult to analyse this liquid with the use of the defocused electron beam (Fig. 4E). That is why the real composition of the sulfide liquid produced by partial melting of the sample FS2-3 is probably more S-rich and Fe-poor than our microprobe results due to the inclusion of primary Fe–Ir–Pt alloys in the analysed volume; the Pt and Ir contents of the liquid being, however, below the microprobe detection limit.

We are confronted with the same problem of an overestimated Fe-content when analysing the composition of the sulfide liquid produced in the Pd-bearing sample FS5-3. During partial melting of this sample Pd partitions predominantly into the Cu–Ni-rich sulfide liquid (3.5 wt.% Pd) and does not form stable Pd-bearing alloys in contrast to Pt and Ir (Table 5). On quenching this Pd-rich liquid solidifies producing many grains of Fe–Ni–Pd alloy intimately mixed, but heterogeneously distributed with other products of solidification hampering the use of a defocused beam (Fig. 4F). That is why the real composition of this liquid is also most likely poorer in Fe and richer in S than our microprobe results (Table 5). As the base–metal starting composition of the Pd-doped sample FS5-3 is almost the same as the Pt–Ir-doped sample FS2-3, the S-content of the sulfide melt in the sample FS5-3 after fS_2 buffering experiments most likely was close to that of the liquid existing in the sample FS2-3, therefore the "Mss-liquid" tie-line for the sample FS5 in Fig. 1 should rotate counter clockwise from the line 1 to the line 2.

The Pd concentration of the Fe-rich monosulfide solid-solution formed during partial melting together with the Cu–Ni–Pd-rich liquid was below the detection limit by microprobe (< 880 ppm). In these experiments the sulfur fugacity did not fall low enough (-6.6 in $\log fS_2$) for a stable Pd alloy to form. The Cu and Ni sample FS7-3 apparently was melted completely after S was lost and all palladium dissolved in the sulfide liquid. In this Cu–Ni-rich part of the system, individual palladium phases did not form either.

3.4. Experiments on solubility of trace quantities of Pt and Ir in the S-poor pyrrhotite

The experiments described above were carried out at the 2000 to 5000 ppm concentration level of PGE in the sulfide assemblages. Concentrations as high as this are found in some PGE reef deposits (Barnes and Maier, 2002; Naldrett, 1989), but most sulfides and more particularly mantle sulfides, contain only 1–100 ppm PGE (Bulanova et al., 1996; Alard et al., 2000). Therefore one could ask whether the present experiments are applicable to natural sulfides.

The low solubility of platinum-group elements in S-poor pyrrhotite or Mss is well known (Li et al., 1996; Ballhaus and Ulmer, 1995; Barnes et al., 2001). Numerous experimental studies report very low or nil Pt and Ir concentrations in Fe-rich, S-poor

base–metal sulfides at conditions of low sulfur fugacity (Ballhaus and Ulmer, 1995; Sinyakova et al., 1996; Makovicky and Karup-Møller, 1999; Majzlan et al., 2002; Peregoedova and Ohnenstetter, 2002). Nevertheless, due to the relatively high detection limit of the electron microprobe used in most of these studies we still do not know how much PGE can be dissolved in the pyrrhotites with the lowest S contents.

To determine at what level pyrrhotite becomes saturated with PGE phases, we conducted high temperature experiments involving the addition of trace quantities, 10–1000 ppm, of Pt or Ir to a S-poor pyrrhotite with a composition approaching stoichiometric FeS. It was found that even when 10 ppm of either Pt or Ir were added into the pyrrhotite, Pt- or Ir-bearing phases, presumably alloys, formed. They were easily detected in the matrix of pyrrhotite under the optical microscope as well as on the electron microprobe in back-scattered images by their brightness and high relief. The compositions of the Pt- or Ir-phases coexisting with S-poor pyrrhotite are presented in the Table 7. Due to the extremely low amount of Pt and Ir added the size of the platinum and iridium phases dispersed in the pyrrhotite matrix was miniscule, making it impossible to perform precise microprobe analysis. Nevertheless, elevated Pt and Ir contents were detected in the vicinity of the alloy grains. In contrast, PGE concentrations were below the detection limit when analysing alloy-free areas of the pyrrhotites. The compositions of alloys were then recalculated assuming that all sulfur in these analyses belongs to the pyrrhotite matrix. These results are only approximate, but they show that when alloys form in association with S-poor pyrrhotite Pt and Ir partition preferentially into the alloys even if only trace quantities of PGE are present. We did not observe any additional sulfide phases attached to the grains of PGE-bearing alloys or textures typical of quenched liquids, thus the alloys do not appear to be products of solidification from a liquid coexisting with Po (cf., Craig and Scott, 1974). However, such a possibility should not be excluded completely. We realize also that alloy formation could happen in this case because of saturation of pyrrhotite with Fe, but it does not change the main conclusion: the results of our experiments of higher PGE concentrations are valid for trace quantities of PGE as the reduction of sulfur fugacity results in an increase in the metal/S ratio of pyrrhotite and if this is high enough for metal saturation to occur Pt and Ir will partition into the alloy.

4. Discussion

At high temperatures (800–1180 °C), S-rich pyrrhotite dissolves large quantities of Pt (1.1 at.%), Ir (1–5.8 at.%) and Os (0.3–0.7 at.%) (Makovicky and Karup-Møller, 1999; Karup-Møller and Makovicky,

Table 7
Results of experiments with 10–1000 ppm of Pt and Ir added in the Po-liquid at 1250 °C

Run#	Composition, wt.%				Run#	Composition, wt.%			
	Fe	Pt	S	Total		Fe	Ir	S	Total
Mc-2					Mc-3				
Starting compositions	63.46	0.10	36.44		Starting compositions	63.45	0.10	36.45	
q-Po	64.27 (0.26)	<0.06	36.24 (0.15)	100.52	q-Po	64.3 (0.28)	<0.07	36.3 (0.11)	100.63
q-alloy[a]	57.1	27.5	14.7	99.3	q-alloy[a]	56.8	28.7	20.2	105.7
Corrected q-alloy	53	47			Corrected q-alloy	42	58		
Mc-4					Mc-6				
Starting compositions	63.52	0.001	36.48		Starting compositions	63.51	0.01	36.48	
q-Po	64.32 (0.16)	<0.06	36.31 (0.1)	100.65	q-Po	64.07 (0.23)	<0.07	36.18 (0.11)	100.27
q-alloy[a]	69	3	30	102	q-alloy[a]	78.2	10.5	14.9	103.6
Corrected q-alloy	72	28				74.6	16.1	15.2	105.8
					Corrected q-alloy	79	21		

The composition of q-alloy was corrected with the use of the matrix composition assuming that the q-alloy does not contain any sulfur; "<0.06"—below the detection limit of the electron microprobe; numbers in parentheses are standard deviations.

[a] Matrix of quench pyrrhotite (q-Po) was included due to the small size (~ 1 μm) of grains of quench alloy (q-alloy).

2002; Majzlan et al., 2002). Ballhaus and Ulmer (1995) reported that (1) maximum solubilities of Pt and Pd in $Fe_{1-x}S$ at 810 °C are about 0.2 and 2.7 at.%, respectively; (2) concentrations of both Pt and Pd fall exponentially with decreasing fS_2 and (3) Pt and Pd initially dissolved in Mss will be exsolved as the Mss recrystallizes to $Fe_{1-x}S$ and pentlandite during cooling to form their own discrete PGE phases. Peregoedova and Ohnenstetter (2002) found that at intermediate temperatures, 760 °C, Pd and Rh dissolve in base–metal sulfide solid-solutions, especially in quaternary solid-solution Hz-Iss and to a lesser extent in Mss, but exsolve from them in the form of individual phases, sulfides or alloys, at lower temperatures. The present experiments confirm that an S-rich (≈ 53 at.%) monosulfide solid-solution can concentrate significant amounts of platinum, iridium and palladium in solid-solution at high temperatures (at least 0.2 wt.%). In addition, our experiments demonstrate that PGE exsolution from sulfides in the form of individual minerals is not always a low-temperature phenomenon, but can easily take place at magmatic temperatures. Thus, we found that at 1000 °C S loss from the monosulfide solid-solution can produce: (1) the exsolution of Pt and Ir from Mss in the form of PGE-bearing alloys, and (2) partial melting of the Cu–Ni-bearing monosulfide solid-solution to form S-poor Mss, Cu–Ni–Pd-rich liquid and Fe–Ir–Pt alloys. Both these events are geologically extremely important.

For example, Lorand and Conquéré (1983) interpreted Cu–Ni-rich interstitial sulfides in spinel lherzolite xenoliths from the Massif Central and Languedoc, France, as having evolved under conditions of desulfurization followed by partial melting of sulfides initially dominated by monosulfide solid-solution. In the present paper we showed experimentally that this model works, and that at magmatic temperatures S loss from the sulfide leads to its partial melting producing Cu–Ni-rich liquid. Ebel and Naldrett (1997) reported that copper strongly influences the transport properties of sulfide liquid. As the copper content of the liquid increases the liquid becomes less viscous, and the diffusivity of metals or metal–sulfide complexes increases in the liquid. Therefore, highly mobile Cu–Ni liquid could migrate away from the more refractory Fe-rich Mss yielding the two kinds of sulfides observed in the mantle (Lorand and Conquéré, 1983; Dromgoole and Pasteris, 1987; Szabó and Bodnar, 1995; Alard et al., 2000, and references therein). Mss residue can be considered as "a high-temperature precursor" of a relatively S- and Fe-rich mantle sulfide assemblage composed of Mss ± minor Cp and Pn with Cu–Ni-rich liquid being "a high-temperature precursor" of an S-poor sulfide assemblage composed of Cp + Pn (Szabó and Bodnar, 1995).

In nature, the S-content of Mss could decrease as result of interaction with S-undersaturated fluids, which could be basalt magma rising through the mantle, or interstitial liquid rising through a magma pile (Fig. 5). As we noted before, mantle sulfides generally consist of monosulfide solid-solution enriched in Ni and to a lesser extent in Cu, and their bulk compositions are very close to the boundary with [Mss + Liquid] phase field (Alard et al., 2000). A small decrease in S content is sufficient to reach this boundary and start melting producing a Cu–Ni sulfide liquid enriched in Pt and Pd (PPGE) and Mss residue with high concentrations of IPGE (Ir, Os, Ru and Rh) (Li et al., 1996). At this stage of the partial melting, the Cu–Ni–Pt–Pd-rich partial melts could migrate away from the solid residue thus spatially decoupling IPGE from PPGE as observed in reefs and mantle xenoliths (Alard et al., 2000; Barnes et al., 2001; Lorand and Alard, 2001). In case of more extensive S loss from the system, Mss will melt producing Fe-rich Mss, Cu–Ni–Pd sulfide liquid and Ir–Pt alloys (Fig. 5), which may be responsible for the fractionation of Pd from Ir and Pt that is generally observed in mantle derived melts (Crocket, 2002, and references there in; Luguet et al., 2003).

According to our data, the maximum sulfur fugacity under which Fe–Ir–Pt alloys can crystallize at 1000 °C during the partial melting of the base–metal sulfide is very low, approximately between −6.7 and −7.1 depending on the composition. Almost the same fS_2 conditions are required to form the exsolution-induced PGE alloys. Thus, at natural PGE concentrations, the extraction of Pt and Ir from pyrrhotite or Fe-rich monosulfide solid-solution at 1000 °C could be expected at log fS_2 approaching −6.9 (corresponding to the stability of stoichiometric FeS which does not incorporate significant concentrations of platinum-group elements). The question is whether such a reduction of the sulfur fugacity can occur under

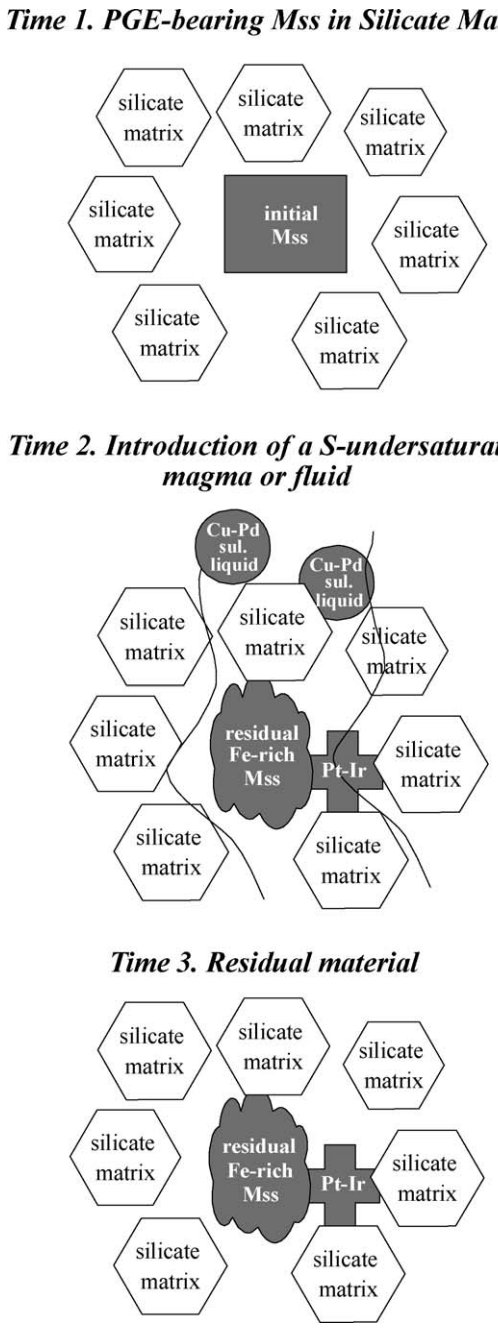

Fig. 5. Model of formation of Pt–Ir alloys from monosulfide solid-solution exposed to desulfurization resulting from sulfide interaction with percolating S-undersaturated melts or fluids.

natural conditions because the fS_2 is linked to fO_2 of magma and the fS_2 calculated here is lower than in most basalt magmas (Wallace and Carmichael, 1992). In our experiments, at $\log fS_2 > -0.9$ all the PGE are dissolved in pyrrhotite. The $\log fS_2$ at which they begin to separate must lie between -6.9 and -0.9. We suggest that PGE exsolution from sulfide solid-solutions could happen at relatively high fS_2 if the base–metal sulfides were particularly enriched in PGE. We observe that PGE start to exsolve from Mss containing about 0.2 wt.% of Pt and Ir when $\log fS_2$ is as high as -1.2 at 980 °C. Additional experiments are necessary to determine the PGE solubility limits for Mss of variable base–metal and S contents.

Another situation where PGE alloys could form from base–metal sulfides is as a consequence of S loss during magma transport. Mantle-derived melts may entrain some sulfide droplets with them (Barnes et al., 2001; Bockrath and Ballhaus, 2002). The solubility of sulfide in basaltic melt increases with decreasing pressure (Mavrogenes and O'Neill, 1999). Thus, during magma ascent the sulfide droplets could be partly resorbed and the S-content of the sulfide liquid could fall sufficiently for alloys to form. However, Andrews and Brenan (2002) suggest that IPGE alloys will not crystallize in sulfide-saturated mafic magmas because of the high solubility of IPGE in a sulfide liquid under fO_2–fS_2 conditions required to maintain sulfide liquid saturation ($\log fO_2 = -9.9$ and $\log fS_2 = -1.6$ at 1200 °C). Moreover, alloy formation appears to require much lower S fugacity, which is difficult to attain as the sulfur fugacity is controlled by fO_2 of the basalt melt and ranges from $\log fS_2$ of -2 to 1 (Wallace and Carmichael, 1992). On the other hand, there is evidence that sulfide liquids coexisting with silicate magmas can have a low S concentration; examples of this are the high metal/S ratios, between 1 and 1.087, recorded in some sulfide globules found in basaltic lavas from mid-oceanic ridges (Czamanske and Moore, 1977). Experimental studies confirm the stability of PGE alloys in S-undersaturated systems of this composition under conditions in which bulk Cu and Ni concentrations do not exceed 4–6 at.% (Fig. 1). Peregoedova and Ohnenstetter (2002) showed that at constant S content of the system, sulfur fugacity increases strongly with increasing Cu and Ni contents. Therefore, sulfide liquids with metal/S ratios close to

1 but richer in Cu and Ni compositions will have higher values of fS_2, apparently too high for PGE alloys to be formed. There is a need for more data concerning fO_2–fS_2 conditions required for alloy saturation in a silicate–sulfide system with variable base–metal and sulfur composition to evaluate the viability of the alloy formation model. Another factor that should be taken into account is the solubility of PGE alloys in the silicate melt. Metal/silicate partition coefficients summarized by Borisov and Palme (2000) are extremely high (10^6–10^{15} at 1350 °C). Moreover, the authors showed that formation of Fe–Pt alloys leads to a significant reduction in the solubility of Pt in a silicate melt, favoring stability of Fe–Pt alloys and fractionation of Pt from Ir and to a lesser extent from Pd.

Another case where the present experiments might be applicable is when sulfide droplets occur in a subvolcanic chamber. Degassing, passive or during eruption, as well as mixing with a sulfide-undersaturated magma will decrease S concentrations in the sulfide droplets. We suggest that this possibly results in the formation of PGM. Larocque et al. (2000) have suggested this leads to Au crystallization. Furthermore, it has been suggested that in chromite-rich portions of the Bushveld reefs sulfides trapped between the chromite grains could lose Fe to the chromite and S to the vapor leaving behind platinum-group minerals crystallized under conditions of low sulfur fugacity (Von Gruenewaldt et al., 1986; Naldrett and Lehmann, 1988; Merkle, 1992; Mathez, 1999; Barnes and Maier, 2002). There are a number of examples of PGE ore deposits where it has been proposed that after sulfides have collected the PGE to form the proto-ore, sulfur was removed by fluids and various metals, including the PGE, dissolved in this fluid (Gain, 1985; Boudreau, 1988; Lavigne and Michaud, 2001). Finally, vapor transport of sulfur and possibly other metals is considered important for formation of some base–metal sulfide deposits (Grinenko, 1985; Ripley and Alawi, 1988; Theriault et al., 2000; Barnes et al., 2001). Initial experiments by Baker et al. (2001) showed that S, Pt, Cu and Ni can be transferred by vapor at 1100 and 1300 °C. Vapor-transport experiments by Peregoedova et al. (2003) revealed that S-dominated vapor could play an important role as a PGE transport agent, especially for palladium.

5. Conclusions

Our experimental study demonstrates that the removal of sulfur from the sulfide by reaction with surrounding minerals or via the vapor phase under conditions of declining sulfur fugacity can produce:

1. The exsolution of Pt and Ir from base–metal sulfides in the form of PGE alloys.
2. Partial melting of the sulfide leading to the formation of S-poor monosulfide solid-solution, Fe–Pt–Ir alloy and highly mobile Cu–Ni–Pd-rich sulfide liquid.

This could separate palladium from platinum and iridium in natural ore systems resulting in the change of the initial Pd/Pt and Pd/Ir ratio.

Idiomorphic PGM crystals do not automatically provide evidence of primary crystallization from liquid. Such crystals may also form by recrystallization of exsolution-induced lamellae of PGM in PGE-bearing base–metal sulfides as a result of sulfur removal from the system, partial melting of sulfide when reducing the sulfur fugacity, or simply cooling.

Acknowledgements

This research was supported by the DIVEX project supported by VRQ (Grant No. 2201-133) and by the Discovery Grants from the Natural Science and Engineering Council of Canada to SJB and to DRB. The authors are thankful to Glenn Poirier and Lang Shi (McGill University) for the assistance with electron-microprobe analyses and to Victoria Pavluchenko (Institut of Mineralogy and Petrology SB RAS) for X-ray diffraction analyses. We gratefully acknowledge referees E. Makovicky, R. Merkle, J. Brenan and the guest editor J.P. Lorand for their constructive comments. [**RR**]

References

Alard, O., Griffin, W.L., Lorand, J.P., 2000. Non-chondritic distribution of the highly siderophile elements in mantle sulphides. Nature 407, 891–894.

Andrews, D.R.A., Brenan, J.M., 2002. The solubility of ruthenium in sulfide liquid: implications for platinum group mineral sta-

bility and sulfide melt-silicate melt partitioning. Chem. Geol. 192, 163–181.

Baker, D.R., Barnes, S.-J., Simon, G., Bernier, F., 2001. Fluid transport of sulfur and metals between sulfide melt and basaltic melt. Can. Mineral. 39, 537–546.

Ballhaus, C., Sylvester, P., 2000. Noble metal enrichment processes in the Merensky Reef, Bushveld Complex. J. Petrol. 41, 545–561.

Ballhaus, C., Ulmer, P., 1995. Platinum-group elements in the Merensky reef: II. experimental solubilities of platinum and palladium in $Fe_{1-x}S$ from 950 to 450 °C under controlled fS_2 and fH_2. Geochim. Cosmochim. Acta 59, 4881–4888.

Barnes, S.-J., Maier, W.D., 2002. The distribution of platinum-group elements in the Merensky Reef, Impala Mines, Western Bushveld Complex. J. Petrol. 43, 103–128.

Barnes, S.-J., Makovicky, E., Makovicky, M., Rose-Hansen, J., Karup-Moller, S., 1997a. Partition coefficients for Ni, Cu, Pd, Pt, Rh, and Ir between monosulfide solid solution and sulfide liquid and the formation of compositionally zoned Ni–Cu sulfide bodies by fractional crystallization of sulfide liquid. Can. J. Earth Sci. 34, 366–374.

Barnes, S.-J., Zientek, M.L., Severson, M.J., 1997b. Ni, Cu, Au, and platinum-group element contents of sulfides associated with intraplate magmatism: a synthesis. Can. J. Earth Sci. 34, 337–351.

Barnes, S.-J., Van Achterbergh, E., Makovicky, E., Li, C., 2001. Proton microprobe results for the partitioning of platinum-group elements between monosulphide solid solution and sulphide liquid. In: Maier, W.D. (Ed.), Platinum Group Elements and Minerals in Southern African Rocks. South Afr. J. Geol., vol. 104, pp. 275–286. Special Issue.

Bockrath, C., Ballhaus, C., 2002. PGE fractionation between sulfide-bearing mantle and basaltic melt during partial melting and melt segregation. 9th International Platinum Symposium, Abstract with Program, 21–25 July 2002, Billings, Montana, 41–43.

Borisov, A., Palme, H., 2000. Solubilities of noble metals in Fe-containing silicate melts as derived from experiments in Fe-free systems. Am. Mineral. 85, 1665–1673.

Boudreau, A.E., 1988. Investigations of the Stillwater Complex: VI. The role of volatiles in the petrogenesis of the J-M Reef, Minneapolis adit section. Can. Mineral. 26, 193–208.

Bulanova, G.P., Griffin, W.L., Ryan, C.G., Shestakova, Ye.O., Barnes, S.-J., 1996. Trace elements in sulfide inclusions from Yakutian diamonds. Contrib. Mineral. Petrol. 124, 111–125.

Cabri, L., Sylvester, P.J., Tubrett, M.N., Peregoedova, A., Laflamme, J.H.G., 2003. Comparison of LAM-ICPMS and MICRO-PIXE analyses for palladium and rhodium in a few samples of Noril'sk and Talnakh sulfides. Can. Mineral. 41, 321–329.

Craig, J.R., Scott, S.D., 1974. Sulfide phase equilibria. In: Ribbe, P.H. (Ed.), Sulfide Mineralogy. Short Course Note, vol. 1. Mineralogical Society of America, Chelsea, MI, pp. CS-1–CS-110.

Crocket, J.H., 2002. Platinum-group elements in basalts from Maui, Hawai'i: low abundances in alkali basalts. Can. Mineral. 40, 595–609.

Czamanske, G., Moore, J.G., 1977. Composition and phase chemistry of sulfide globules in basalt from the Mid-Atlantic ridge rift valley near 37°N lat. Geol. Soc. Am. Bull. 88, 587–599.

Dromgoole, E.L., Pasteris, J.D., 1987. Interpretation of the sulfide assemblages in a suite of xenoliths from Kilbourne Hole, New Mexico. In: Morris, E., Pasteris, J.D. (Eds.), Mantle Metasomatism and Alkalin Magmatism, Special paper, vol. 215. Geological Society of America, Washington, DC, pp. 25–46.

Ebel, D.S., Naldrett, A.J., 1997. Crystallization of sulfide liquids and the interpretation of ore composition. Can. J. Earth Sci. 34, 352–365.

Fleet, M.E., Stone, W., 1991. Partitioning of platinum-group elements in the Fe–Ni–S system and their fractionation in nature. Geochim. Cosmochim. Acta 55, 245–253.

Gain, S.B., 1985. The geologic setting of the platiniferous UG-2 chromitite layer on the Farm Maandagshoek, Eastern Bushveld Complex. Econ. Geol. 80, 925–943.

Grinenko, L.N., 1985. Sources of sulfur of the nickeliferous and barren gabbro dolerite intrusion of the northwest Siberian platform. Intern. Geol. Review 27, 695–708.

Karup-Møller, S., Makovicky, E., 2002. The system Fe–Os–S at 1180 °C, 1100 °C and 900 °C. Can. Mineral. 40, 499–507.

Kullerud, G., Yund, R.A., Moh, G.H., 1969. Phase relations in the Cu–Fe–S, Cu–Ni–S and Fe–Ni–S systems. Econ. Geol. Monogr. 4, 323–343.

Larocque, A.C.L., Stimac, J.A., Keith, J.D., Huminicki, M.A.E., 2000. Evidence for open-system behavior in immiscible Fe–S–O liquids in silicate magmas; implications for contributions of metals and sulfur to ore-forming fields. Can. Mineral. 38, 1233–1250.

Lavigne, M.J., Michaud, M.J., 2001. Geology of North American Palladium's Roby Zone Deposit, Lac des Iles. Explor. Min. Geol. 10 (1–2), 1–17.

Li, C., Barnes, S.-J., Makovicky, E., Rose-Hansen, J., Makovicky, M., 1996. Partitioning of nickel, copper, iridium, rhodium, platinum, and palladium between monosulfide solid solution and sulfide liquid: effects of composition and temperature. Geochim. Cosmochim. Acta 60, 1231–1238.

Lorand, J.P., 1989. Abundance and distribution of Cu–Fe–Ni sulfides, sulfur, copper and Platinum-group elements in orogenic-type spinel lherzolite massifs of Ariège (Northeastern Pyrenees, France). Earth Planet. Sci. Lett. 93, 50–64.

Lorand, J.P., Alard, O., 2001. Geochemistry of platinum-group elements in the sub-continental lithospheric mantle; in-situ and whole-rock analyses of some spinel peridotite xenoliths, Massif Central, France. Geochim. Cosmochim. Acta 65, 2789–2806.

Lorand, J.P., Conquéré, F., 1983. Contribution à l'étude des sulfures dans les enclaves de lherzolites à spinelle des basaltes alcalins (Massif Central et du Languedoc, France). Bull. Minéral. 106, 585–606.

Luguet, A., Lorand, J.P., Seyler, M., 2003. A coupled study of sulfide petrology and highly siderophile element geochemistry in abyssal peridotites from the Kane Fracture Zone (mark area, Mid-Atlantic ridge). Geochim. Cosmochim. Acta 67, 1553–1570.

Majzlan, J., Makovicky, M., Makovicky, E., Rose-Hansen, J., 2002. The system Fe–Pt–S at 1100 °C. Can. Mineral. 40, 509–517.

Makovicky, E., 2002. Ternary and quaternary phase systems with

PGE. In: Cabri, L.J. (Ed.), The Geology, Geochemistry, Mineralogy and Mineral Beneficiation of Platinum-group Elements. Canadian Institute of Mining, Metallurgy and Petroleum, Montreal, Special vol. 54, pp. 131–175.

Makovicky, E., Karup-Møller, S., 1999. The phase system Fe–Ir–S at 1100, 1000 and 800 °C. Mineral. Mag. 63, 379–385.

Makovicky, E., Karup-Møller, S., 2000. Phase relations in the metal-rich portions of the phase system Pt–Ir–Fe–S at 1000 °C and 1100 °C. Mineral. Mag. 64, 1047–1056.

Makovicky, M., Makovicky, E., Rose-Hansen, J., 1986. Experimental studies on the solubility and distribution of platinum group elements in base–metal sulphides in platinum deposits. In: Gallagher, M.J., Ixer, R.A., Neary, C.R., Prichard, H.M. (Eds.), Metallogeny of Basic and Ultrabasic Rocks. The Institution of Mining and Metallurgy, London, UK, pp. 415–425.

Makovicky, M., Makovicky, E., Rose-Hansen, J., 1988. Experimental evidence of the formation and mineralogy of platinum and palladium ore deposits. In: Boissonnas, J., Omenetto, P. (Eds.), Mineral Deposits within the European Community. Springer-Verlag, Berlin, Germany, pp. 303–317.

Makovicky, E., Karup-Møller, S., Makovicky, M., Rose-Hansen, J., 1990. Experimental studies on the phase systems Fe–Ni–Pd–S and Fe–Pt–Pd–As–S applied to PGE deposits. Mineral. Petrol. 42, 307–319.

Mathez, E.A., 1999. On factors controlling the concentrations of platinum group elements in layered intrusions and chromitites. In: Keays, R.R., Lesher, C.M., Lightfoot, P.C., Farrow, C.E.G. (Eds.), Dynamic Processes in Magmatic Ore Deposits and Their Application to Mineral Exploration. Geological Association of Canada, Short Course Notes, vol. 13, pp. 251–285.

Mavrogenes, J.A., O'Neill, H.St.C., 1999. The relative effects of pressure, temperature and oxygen fugacity on the solubility of sulfide in mafic magmas. Geochim. Cosmochim. Acta 63, 1173–1180.

Merkle, R.K.W., 1992. Platinum-group minerals in the middle group of chromitite layers at Marikana, Western Bushveld Complex: indications for collection mechanisms and postmagmatic modification. Can. J. Earth Sci. 29, 209–221.

Naldrett, A.J., 1967. Partial pressure of sulfur in the vapor coexisting with the $Fe_{1-x}S$–$Ni_{1-x}S$ solid solution at 600 °C. Annual Report of the Director Geophysical Laboratory 1965–1966. Carnegie Institution, Washington, pp. 326–328.

Naldrett, A.J., 1989. Magmatic Sulfide Deposits. Clarendon Press, New York, NY.

Naldrett, A.J., Lehmann, J., 1988. Spinel non-stoichiometry as the explanation for Ni-, Cu-, and PGE-enriched sulfides in chromitites. In: Prichard, H.M., Potts, P.J., Bowles, J.F.W., Cribb, S.J. (Eds.), Geo-Platinum, vol. 87. Elsevier, London, pp. 113–143.

Pattou, L., Lorand, J.P., Gros, M., 1996. Non-chondtritic platinum-group element ratios in the Earth's mantle. Nature 379, 712–715.

Peregoedova, A.V., Ohnenstetter, M., 2002. Collectors of Pt, Pd and Rh in a S-poor Fe–Ni–Cu–sulfide system at 760 °C: experimental data and application to ore deposits. Can. Mineral 40, 527–561.

Peregoedova, A., Barnes, S.-J., Baker, D., 2003. Transport of platinum-group elements in a S-dominated vapor at magmatic temperatures. GSA Abstracts with Programs, 2–5 November 2003, Seattle, Washington, p. 231.

Ripley, E.M., Alawi, J.A., 1988. Petrogenesis of pelitic xenoliths at the Babbitt Cu–Ni deposit, Duluth Complex, Minnesota, USA. Lithos 21, 143–159.

Sinyakova, E.F., Fedorova, Zh.N., Pavluchenko, V.S., 1996. Physical–chemical conditions of formation of platinum phases in the system Fe–Ni–S. Geol. Geofiz. 37, 39–49 (English Transl. Russ. Geol. Geophys. 37, 38–48).

Szabó, Cs., Bodnar, R.J., 1995. Chemistry and origin of mantle sulfides in spinel peridotite xenoliths from alkaline basaltic lavas, Nógrád-Gömör Volcanic Field, northern Hungary and southern Slovakia. Geochim. Cosmochim. Acta 59, 3917–3927.

Theriault, R.D., Barnes, S.-J., Severson, M.J., 2000. Origin of Cu–Ni–PGE sulfide mineralization in the Partridge River Intrusion, Duluth Complex, Minnesota. Econ. Geol. 95, 929–943.

Toulmin III, P., Barton Jr., P.B. 1964. A thermodynamic study of pyrite and pyrrhotite. Geochim. Cosmochim. Acta 28, 641–671.

Von Gruenewaldt, G., Hatton, C.J., Merkle, R.K.W., Gain, S.B., 1986. Platinum-group element–chromitite associations in cumulates of the Bushveld Complex. Econ. Geol. 81, 1067–1079.

Wallace, P., Carmichael, I.S.E., 1992. Sulfur in basaltic magmas. Geochim. Cosmochim. Acta 56, 1863–1874.